doi:10.26443/seismica.v2i2.1082

Passive Assessment of Geophysical Instruments Performance using Electrical Network Frequency Analysis

M. R. Koymans * [1,2], **J. D. Assink** [1], **E. de Zeeuw-van Dalfsen** [1,3], **L. G. Evers** [1,2]

[1]Department of Seismology and Acoustics, Royal Netherlands Meteorological Institute, Utrechtseweg 297, De Bilt 3731 GA, Utrecht, the Netherlands, [2]Geoscience and Engineering, Delft University of Technology, Stevinweg 1, Delft 2628 CN, Zuid-Holland, the Netherlands, [3]Geoscience and Remote Sensing, Delft University of Technology, Stevinweg 1, Delft 2628 CN, Zuid-Holland, the Netherlands

Author contributions: *Conceptualization*: Mathijs Koymans. *Methodology*: Mathijs Koymans. *Software*: Mathijs Koymans. *Validation*: Mathijs Koymans, Jelle Assink, and Läslo Evers. *Writing - Original draft*: Mathijs Koymans. *Writing - Review & Editing*: Jelle Assink, Elske de Zeeuw-van Dalfsen, and Läslo Evers. *Supervision*: Elske de Zeeuw-van Dalfsen and Läslo Evers.

Abstract The electrical network frequency (ENF) of the alternating current operated on the power grid is a well-known source of noise in digital recordings. The noise is widespread and appears not just in close proximity to high-voltage power lines, but also in instruments simply connected to the mains powers grid. This omnipresent, anthropogenic signal is generally perceived as a nuisance in the processing of geophysical data. Research has therefore been mainly focused on its elimination from data, while its benefits have gone largely unexplored. It is shown that mHz fluctuations in the nominal ENF ($50/60$ Hz) induced by variations in power usage can be accurately extracted from geophysical data. This information represents a persistent time-calibration signal that is coherent between instruments over national scales. Cross-correlation of reliable reference ENF data published by electrical grid operators with estimated ENF data from geophysical recordings allows timing errors to be resolved at the 1 s level. Furthermore, it is shown that a polarization analysis of particle motion at the ENF can detect instrument orientation anomalies. While the source of the ENF signal in geophysical data appears instrument and site specific, its general utility in the detection of timing and orientation anomalies is presented.

Production Editor: Gareth Funning
Handling Editor: Catherine Rychert
Copy & Layout Editor: Hannah F. Mark

Received: July 6, 2023
Accepted: November 6, 2023
Published: December 12, 2023

1 Introduction

Sustaining reliable and continuous operation of instruments in the field is a key objective in the maintenance of geophysical monitoring infrastructures. This objective is particularly challenging for remote deployments, and equipment that cannot easily be accessed, e.g., for sensors buried at depth inside seismic boreholes. Active assessments that involve station maintenance visits are costly, time-consuming, and require perpetual planning and effort. Methods for passive quality assessment are often pursued due to their advantages in terms of scalability and reduced cost (McNamara and Boaz, 2006; Ahern et al., 2015; Ringler et al., 2015; Trani et al., 2017; Petersen et al., 2019; Pedersen et al., 2020; Koymans et al., 2021). Moreover, such passive techniques do not disturb the measurement setup itself and may be useful in, e.g., citizen science (Raspberry Shake, S.A., 2016) where the acquisition of high quality data can not be guaranteed. In the case where correction factors can be estimated, they can also be retroactively applied to an archived dataset. Data assessment is not exclusively useful to science, but also serves a purpose to detect malicious actors and data tampering that is critical in, e.g., the verification of the Comprehensive Nuclear-Test-Ban Treaty (Coyne et al., 2012).

Geophysical data may express characteristic spectral peaks that emerge from the electrical network frequency (ENF) of the alternating current (AC) operated on the electrical grid. This signal is sometimes referred to as *powerline* noise, but notably does not appear exclusively near high voltage power lines and is widespread. The signal is omnipresent in recordings from, e.g., seismometers (Bormann and Wielandt, 2013), gravimeters (Imanishi et al., 2022; Křen et al., 2021), microbarometers, and other digital instruments that are connected to or deployed near any type of electrical infrastructure or mains power supply. The ENF signal is usually perceived as a nuisance during the processing of geophysical data, and research has mainly been targeting its elimination (Butler and Russell, 1993; Xia and Miller, 2000; Levkov et al., 2005). For most purposes, the application of a narrow band-stop (notch) filter is sufficient to remove the signal. However, ringing artefacts, higher harmonics, or overlap with the bandwidth of interest sometimes makes the application of such filters impractical. For example, in seismoelectric acquisition and seismic exploration, advanced methods for the removal of coherent electrical noise are applied (Butler and Russell, 1993, 2003). While methods to eliminate the ENF signal from geophysical data are well known,

*Corresponding author: koymans@knmi.nl

the benefits of its presence are rarely explored. This study approaches the ENF from a different perspective, and demonstrates its utility as a signal in geophysics.

In this manuscript, two benefits of detecting the ENF in geophysical data are explored and used as passive quality assessment tools. First, the background information on the ENF is described (section 2), followed by an introduction of the data sets that are used (section 3.1). After that, the methodologies are described to **(i)** extract the ENF signal from spectrograms of geophysical data (section 3.2) and compute cross correlations (section 3.3), and **(ii)** complete a polarization analysis of the particle motion around the ENF (section 3.4). Results from cross correlations between spectrogram-estimated and reference ENF data are presented, demonstrating that timing errors with a resolution near the $1\,\mathrm{s}$ level can be resolved and verified (section 4.1). The accuracy of the recovered timing discrepancies are statistically quantified (section 4.2.1) and checked using teleseismic arrivals (section 4.2.2) that should be observed simultaneously on stations in close proximity, providing an alternative way of detecting relative time shifts. Results from the polarization analysis indicate that the method is capable of detecting gross sensor orientation anomalies (section 4.3). Finally, the source of the ENF signal in different geophysical instruments is discussed, and comments are provided on possible future avenues of research (section 5).

2 Background

2.1 Electrical Network Frequency

An abridged description of the electrical grid concerns power generators that supply electrical energy to consumers. Conceptually, generators are rotating turbines with magnetic cores that induce AC in coils following Faraday's law of electromagnetic induction. All generators on the grid collectively produce synchronous AC, with waveforms that are equal in amplitude, phase, and frequency. Because the electrical energy produced by the generators cannot be stored it must be immediately consumed, requiring a delicate balance between production and demand. At an instant when more energy is consumed than produced, the required excess power is drawn from the rotational inertia of the generators. This synchronously reduces the rotation speed of the generators on the grid, and subsequently lowers the effective ENF. Likewise, a sudden decrease in load causes the turbines to spin faster, leading to an increase of the ENF. Electrical grid operators balance the amount of electrical work done by the generators with the demand of consumers to keep the ENF stable at $50\,\mathrm{Hz}$ for continental Europe and $60\,\mathrm{Hz}$ for the United States. This balance is diligently maintained, and operational procedures are in place to limit deviations from the target ENF to within 10 to $50\,\mathrm{mHz}$.

All electrical components – including geophysical instruments – are to some degree susceptible to the secondary effects of the AC operated on the electrical grid (fig. 1). Signals may be incurred from stray electromagnetic fields that are emitted from nearby current carrying wires and operating electronics. Common sources of the ENF signal being carried over in electric devices are through ground loops, and by direct electromagnetic induction of poorly shielded wires and circuitry. Magnetostriction in transformers (Gange, 2011) and full-bridge rectifiers (AC $\rightarrow$ DC) in power supplies may produce vibrations and audible sound at double the ENF. The well-known audible sound originating from the ENF is commonly referred to as *mains hum*. In broadband seismometers, a known coupling mechanism is through the suspension spring that responds to changing magnetic fields (Forbriger, 2007). Intense changing magnetic fields may even cause the housing of instruments to vibrate (Klun et al., 2019). At frequencies above the operated ENF, overtones at integer multiples of the ENF can sometimes be observed (Cohen et al., 2010; Schippkus et al., 2020).

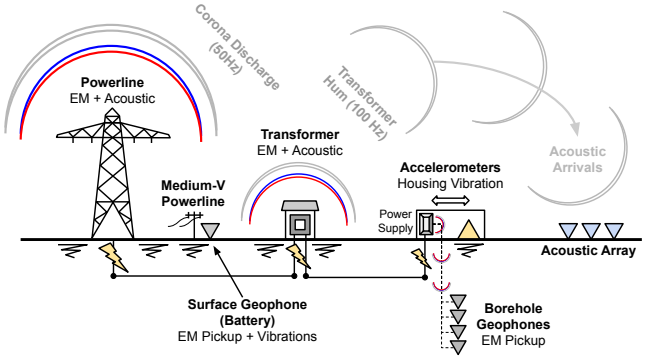

Figure 1 Overview of suspected sources of the ENF signal in geophysical data where the colors represent electromagnetic (red/blue), acoustic (grey), and seismic (black) coupling. The coupling mechanism varies between instruments and installation site. The signal may be coupled through physical vibrations, acoustic waves, or by direct magnetic induction.

While the ENF signal is typically of minor influence, equipment that integrates amplifiers may boost it to significant amplitudes. While the source of the ENF signal in high gain equipment is not always directly apparent from its surrounding, its persistence and omnipresence remains remarkable.

2.2 ENF Analysis

ENF analysis typically concerns the detection of mHz variations of the ENF in digital recordings as a function of time, of which an example is illustrated in fig. 2. These variations can be extracted from, e.g., audio (Cooper, 2008), optical (Garg et al., 2011), and geophysical data (Cohen et al., 2010). Because the AC is operated synchronously and uniformly on the electrical grid, digital recordings of the ENF represent a fingerprint that is coherent nationwide and, because of effectively random load fluctuations, represents a signal that is unique in time. The estimated variations in the ENF from digital recordings may thus be compared to an independent reliable reference measurement of the ENF that is provided by electrical grid operators. Such analysis of the ENF has been used to timestamp audio recordings (Garg et al., 2012) and confirm the authenticity of digital

records. The successful use of ENF analysis as forensic evidence (Cooper, 2010) is a testament to the effectiveness and reliability of the technique.

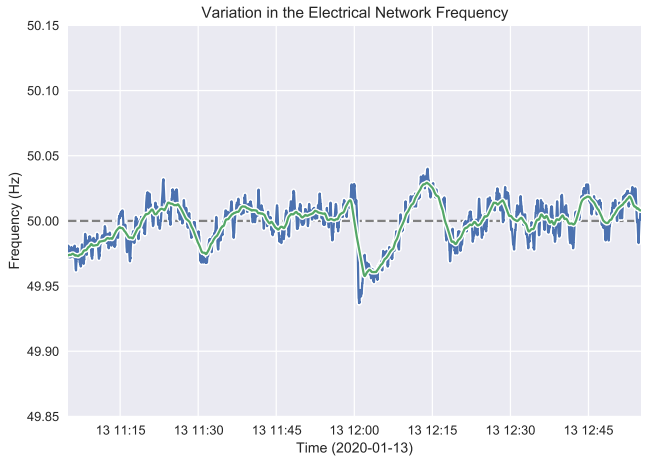

Figure 2 Example of minor mHz variations in the ENF during two minutes on Jan 13th, 2020 around the nominal European grid frequency of 50 Hz (grey dashed line). These data were not recorded by a geophysical instrument but illustrate reference ENF data that were downloaded from electrical grid operator TransnetBW. The raw data are plotted in blue, with a smoothed 150 s moving average illustrated in green.

3 Methodology

3.1 Instruments and Data Used

Various data types from different sensors are analysed in order to study the specific character of the ENF in these instruments. Data from the Netherlands Seismic and Acoustic Network (KNMI, 1993) and E-TEST temporary deployment (Shahar Shani-Kadmiel et al., 2020) (fig. 3 and table 1) are treated. The G-network of the Netherlands Seismic and Acoustic Network (NSAN) consists of nearly seventy 200 m deep boreholes in the Groningen province with geophones installed at 50 m depth intervals, and an accelerometer located at the surface. Data from the NSAN that belong to a low-frequency acoustic array installed at the Royal Netherlands Meteorological Institute in De Bilt (see supplementary information), and seismo-acoustic arrays at LOFAR sites in Drenthe are also analysed. The E-TEST temporary deployment consists of a dense array of battery-operated surface geophones located in the south of the province of Limburg without a main power supply.

3.2 Spectrogram Calculation and ENF Estimation

Independent ENF reference measurements at 1 Hz are universally accessible and downloaded from, e.g., the power-grid frequency database (Gorjão et al., 2020) and the website of TransnetBW GmbH. In this manuscript, ENF measurements from a German provider were used – data that are synchronous with the electrical grid operated in the Netherlands. The reference ENF data were smoothed using a centered moving average filter over 150 s (e.g., see fig. 2).

Geophysical data from the instruments summarised in table 1 were pre-processed using ObsPy (Beyreuther et al., 2010) (read and merged) and spectrograms were calculated using the SciPy *spectrogram* method (Virtanen et al., 2020) with a segment length of 150 s, employing a 50 % overlap between consecutive segments. It was determined empirically that this segment length provided the most effective trade-off in resolution between time and frequency to resolve the ENF from the spectrograms. A linear trend was removed from each segment and the data were tapered using a cosine window with a shape parameter of 0.25. A Gaussian filter was applied in the frequency domain before the ENF was estimated from the spectrogram. This filter represents the mean and standard deviation of the yearly ENF signal ($\mathcal{N}_{50}(\mu,\,\sigma) = 50.000\,\mathrm{Hz}, 441 \times 10^{-4}\,\mathrm{Hz}$), and eliminates peaks in the spectrogram that are likely unrelated to the ENF. For each segment, the estimated ENF is represented by the frequency bin that associates with the maximum PSD within the 49.85 to 50.15 Hz band. An identical approach (with modified filter $\mathcal{N}_f$) was used for the extraction of overtones of the ENF in higher frequency bands (e.g., at 100 Hz).

3.3 Cross-Correlation Analysis

The estimated variations in the ENF were interpolated to 1 s and cross-correlated with independent reference ENF data. A negative delay from the cross-correlation result implies that the reference signal leads the estimated ENF and is therefore behind *true* time. A statistical analysis of the accuracy and precision of the method was completed using an ensemble of cross correlations from instruments that are known to have zero time delay. The accuracy of the method and the recovered timing errors were further verified at a seismic array using teleseismic arrivals from an event near the Kermadec Islands, New Zealand (2021-03-04T19:28:33 UTC). Because the teleseismic arrivals are characterised by a near vertical incidence angle, the arrival times for proximal stations are expected to be similar, providing an alternative relative timing reference to compare against the obtained ENF analysis results.

3.4 ENF Polarization Analysis

Another independent aspect where the ENF signal can be leveraged is for surface accelerometers in the G-network that express a significant and strongly polarized susceptibility to the ENF. Accelerometer data were rotated towards a north-east orientation following the azimuth provided by the station metadata. The polarized ENF signal was isolated with a zero-phase band-pass filter between 49.85 to 50.15 Hz. A principal component analysis (PCA) was applied to the three-dimensional particle motion data and eigenvalues (λ_1, λ_2, λ_3) were recovered, from which the degree of rectilinearity (Jurkevics, 1988) was calculated:

Sensor	Description	Network	Sampling Rate
SM6H	Borehole geophone	G-network (NL)	200
Kinemetrics EpiSensor (ES-T)	Strong-motion accelerometer	G-network (NL)	200
SM-6/U-B 4.5Hz 375	Sensor B.V. Geophone	LOFAR Array (NL)	250
Hyperion Infrasound Sensor	Low-frequency sound microphone	De Bilt Array (NL)	500
SENSOR Nederland, PE-6/B, 3C	Battery operated geophone	E-TEST Deployment (3T)	500

Table 1 Descriptions and characteristics of geophysical instruments used for various aspects of ENF analysis that are treated in this manuscript and supplementary material. Instrument and response details are accessible from FDSN webservices (http://rdsa.knmi.nl and http://orfeus-eu.org).

$$1 - \left(\frac{\lambda_2 + \lambda_3}{2\lambda_1} \right) \tag{1}$$

The azimuth of the principal direction of motion (θ) was derived from the largest eigenvector $\mathbf{u}_1$, as given by its north and east components: $\theta = \arctan_2(\mathbf{u}_{1_N}, \mathbf{u}_{1_E})$. The goal of this method is to investigate whether the ENF can be used to verify the instrument orientation as specified in the station metadata.

4 Results

4.1 Timing Errors from ENF Analysis

An example ENF analysis for instrument EpiSensor accelerometer G180 is shown in fig. 4. The figure illustrates the reference variation in the ENF around $50\,\mathrm{Hz}$ (A), the raw seismometer spectrogram expressed in ground acceleration (B), the spectrogram with the Guassian filter applied (C), and that the ENF can be accurately recovered from the filtered spectrogram (D). fig. 5 panel A shows the measured and estimated ENF time series from fig. 4. The curves were vertically displaced from an average of $50\,\mathrm{Hz}$ to illustrate their similarity. The full cross-correlation of the measured and estimated ENF is illustrated in panel B and expresses a peak at a delay of $-1\,\mathrm{s}$ (C), meaning the instrument effectively runs behind *true* time. An identical analysis for an acoustic station is presented in the supplementary information because of additional complications that were encountered.

The presented example result in figs. 4 and 5 illustrates the method for a single instrument, but the approach has been successfully applied to all instruments in the NSAN network, including surface accelerometers, geophones, and microbarometers. The results indicate that the proposed method appears capable of detecting misfits between the estimated and reference ENF in geophysical data, potentially providing a stable nationwide timing calibration signal.

4.2 Validation of Timing Error Results

In the following sections, two methods are used to assess the precision and accuracy of the proposed method for the detection of timing anomalies.

4.2.1 Resolution of the Method

An estimate of the statistical significance of the recovered time lags is obtained through an ensemble of cross correlations between the measured and estimated ENF from all components of 71 surface accelerometers in the NSAN. These instruments are known to have accurate timestamps because they obtain timing through GPS and should thus express a zero-second delay from true time. fig. 6 shows an ensemble of 211 cross correlations with its average and $95\,\%$ confidence interval in blue. The peaks of all cross correlations and recovered time lags are also illustrated by grey markers. Accelerometers for which the ENF could not be resolved due to poor data quality or elevated noise have been removed from the ensemble. The majority of instruments express a lag of $-1\,\mathrm{s}$ between the estimated and measured ENF data, while the others express a $0\,\mathrm{s}$ time lag as expected. The confidence interval on the mean time lag from this ensemble illustrates the estimated accuracy and precision of the method at approximately $1\,\mathrm{s}$. Furthermore, the repeatability of the methodology between 211 data channels is a testament to its consistency. The minor stable deviation from the expected delay of zero may be caused by a non-precise or rounded off timestamp of the ENF data provided by the grid operator.

4.2.2 Verification Using Teleseismic Arrivals

The accuracy of the recovered timing errors was further verified using teleseismic arrivals at geophone ENV1 and nearby LOFAR arrays L106 and L208 of the M8.1 earthquake near the Kermadec Islands, New Zealand that occurred at 2021-03-04T19:28:33 UTC. The first two rows of fig. 7 show station ENV1 and L2082 at $24\,\mathrm{km}$ and $13\,\mathrm{km}$ distance from LOFAR array L106 (bottom 6 rows) respectively. The predicted seismic arrival times for the PKIKP phase of the event were calculated with TauPy (Beyreuther et al., 2010) using the IASP91 model (Kennett and Engdahl, 1991). The left column in fig. 7 shows that the recorded arrivals of the seismic phase of the original time-series are misaligned. The right panels show the same data shifted by the recovered delay from the ENF analysis (marked in the top-left corner of each panel). Geophone ENV1 and LOFAR station L2081 acquire timing through GPS and have near zero delay, while the L106 geophones express between -21 to $-7\,\mathrm{s}$ delays with the reference ENF. This effect is unsurprising as the instruments use the Network Time Protocol (NTP) instead of GPS and may experience clock drift over time without a stable internet connection. With the expected timing corrections applied, the alignment of the arrivals is vastly improved. The remaining misalignment may be a consequence of local geology and site-

Figure 3 Map of the Netherlands showing four groups and locations of geophysical instruments in the field (G-Network – geophones and surface accelerometers; E-TEST Deployment – battery operated geophone nodes; LOFAR – seismo-acoustic array; De Bilt – acoustic array). The acoustic instruments are treated in the supplementary material. Further details on the instruments are provided in Table 1.

response, and the inherent 1 s resolution limit of the technique. Furthermore, the timing misfits from the ENF analysis were calculated over 24 h while the timing error of the L106 array was observed to vary by multiple seconds in a day. At the time of the teleseismic arrival, the ENF delay appeared to be consistently 6 s behind the reference data for the entire NSAN network. This effect was corrected in fig. 7 using an average of many GPS

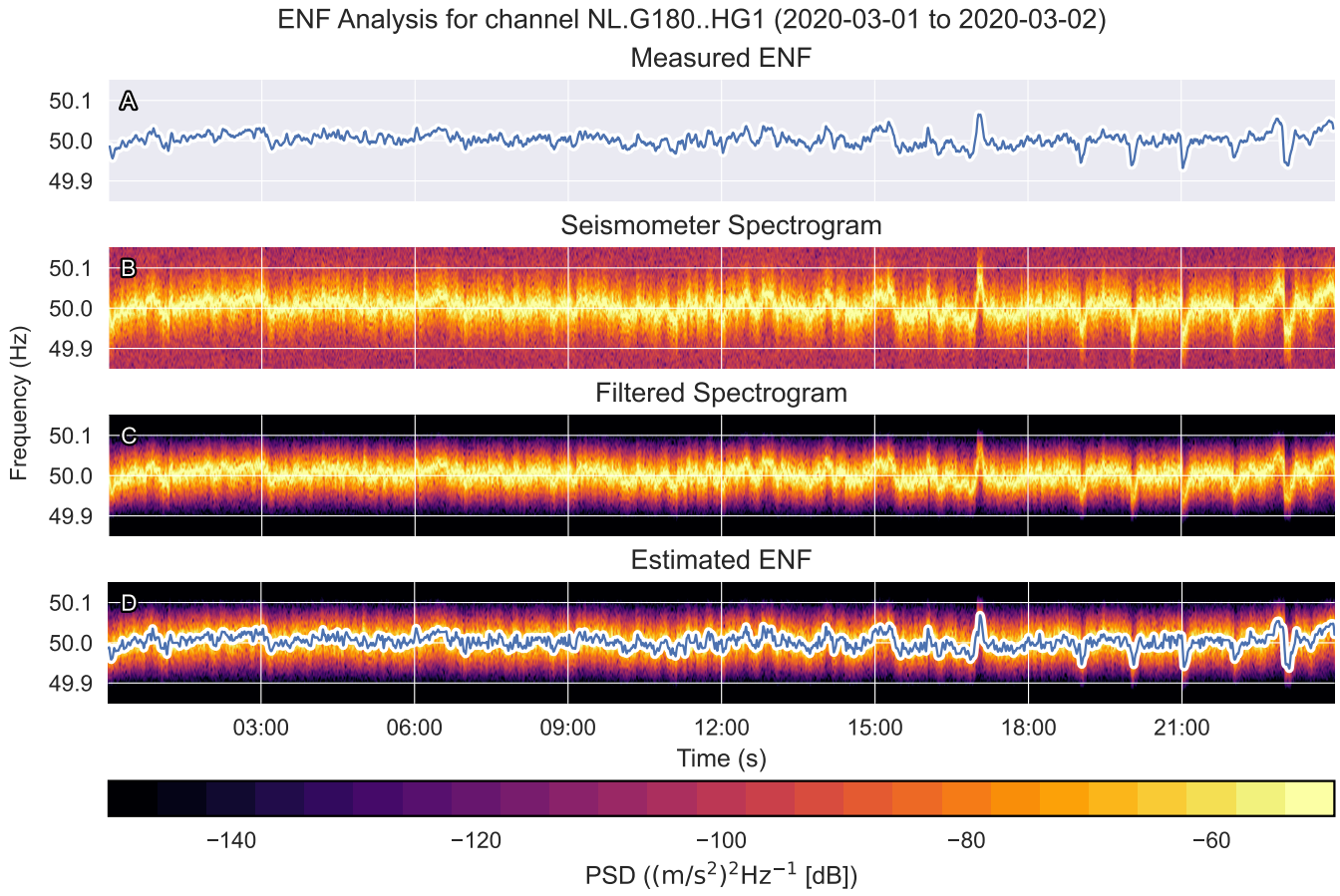

Figure 4 A) The reference ENF downloaded from the website of TransnetBW GmbH. B) Acceleration spectrogram of EpiSensor NL.G180..HG1 (Groningen, the Netherlands) between 2020-03-01 and 2020-03-02. C) The modified spectrogram using a simple Gaussian filter. D) The estimated ENF from the filtered spectrogram derived from the maximum PSD of each time segment.

locked stations.

4.3 Orientation Anomalies from ENF Analysis

A polarization analysis of the ENF signal was applied to three-component data from surface accelerometers in the G-network. A principal component analysis provides the dominant modes of variance of these data (i.e., the dominant direction of motion), of which an example is illustrated for surface accelerometer G450 (fig. 8). The three-component data are plotted together in three-dimensional space and the ground motion (represented by the position of a virtual particle) is projected onto three perpendicular two-dimensional slices. The results show that in the 49.85 to 50.15 Hz frequency band, the ground motion has a high probability of being on the colored elliptical path and not outside or inside of it, where the probability approaches zero.

Because the polarization was observed to be dominantly in the horizontal plane, the recovered azimuths from the polarization analysis (leftmost panel of fig. 8) were projected on geographic maps together with open electrical infrastructure data to identify potential directional sources of the ENF. It was however not possible to identify a regional source of the ENF signal such as medium and high voltage line and transformers. Instead, it was considered that for most instruments, local electronics inside the instrument's housing cabinet may be a more proximal and likely source of the signal. The cabinets that host both the accelerometers and electronics in the G-network is shaped like a rectangular box (ratio 1:3), with the internal setup organised in a similar fashion for all installations. Azimuths of the cabinet in the field (parallel with the elongated side) were estimated from technical drawings. The direction of polarized motion that is expressed by the accelerometer data appears to be consistent with the azimuth of the cabinet (fig. 9, left panel), confirming the source of the ENF is in fact local. The right panel of fig. 9 shows the misfit between the azimuth of particle motion and the cabinet orientation plotted against the degree of rectilinearity. Stations that express a lower degree of rectilinearity naturally have a larger variability on the direction of particle motion, resulting in a more probable angular misfit. The decreased degree of rectilinearity may be attributed to a diminished source of the ENF or instrument sensitivity issues, which can be considered another instrument health metric.

A clear outlier was identified as station G680 marked in that expresses a $87°$ near perpendicular angular misfit with a very strong rectilinearity (fig. 9). It was hypothesised that the instrument was rotated, or that the horizontal components were swapped during instrument installation. A field visit confirmed that surface ac-

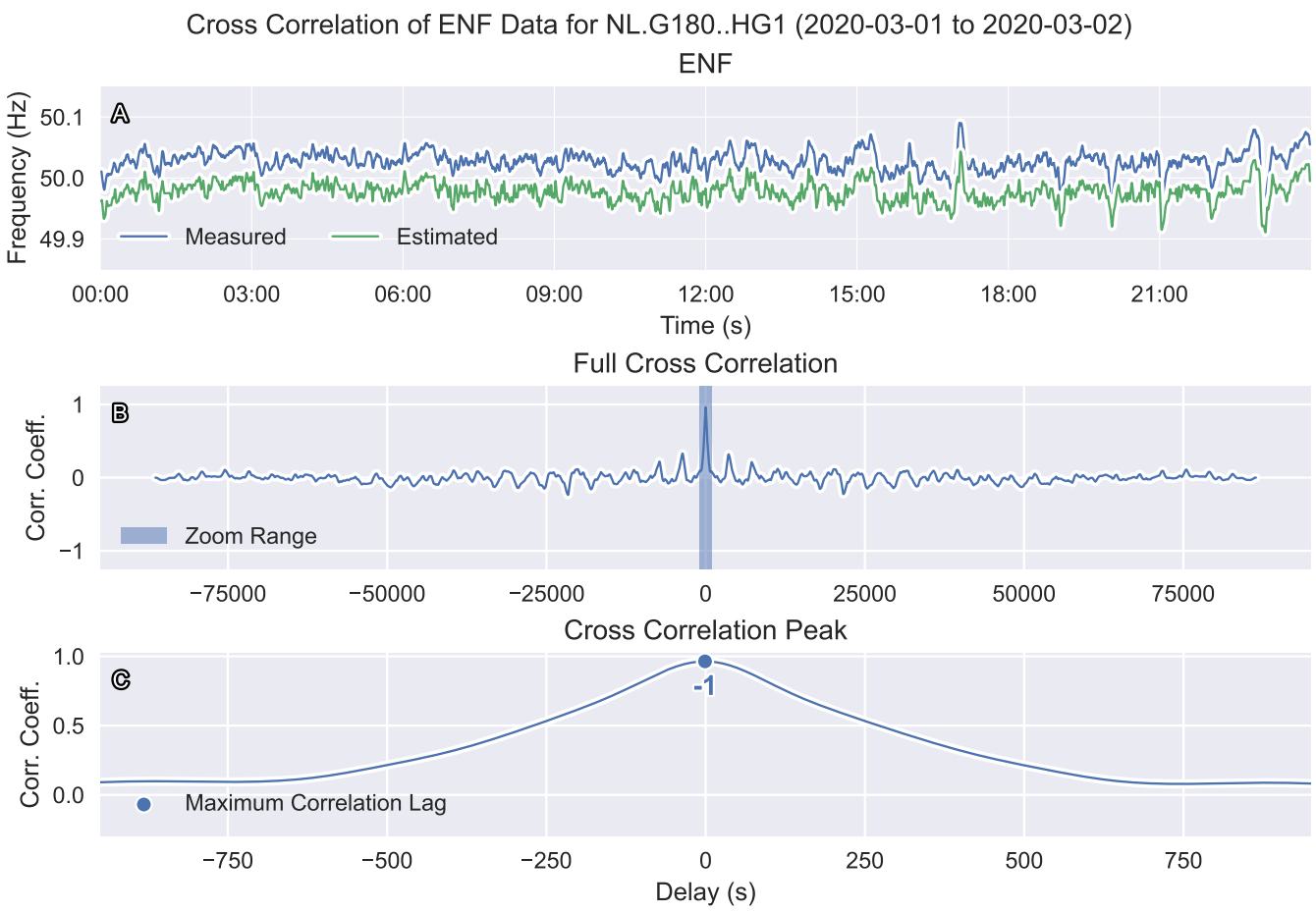

Figure 5 A) Comparison between the reference ENF (blue) provided by TransnetBW GmbH and the estimated ENF (green). Note that the data have been offset from the mean of $50\,\mathrm{Hz}$ for illustrative purposes to show their similarity. B) The full cross correlation between the estimated and reference ENF. C) Zoom in on the blue span around the correlation maximum (≈ 0.96) with the recovered peak and time delay indicated ($-1\,\mathrm{s}$).

celerometer G680 was in fact rotated counter-clockwise by $90°$ and has been corrected since.

5 Discussion

The applied tracing algorithm (fig. 4D) to estimate the ENF from spectrograms using the maximum PSD per time bin is simple yet effective. The intensity of the ENF above ambient noise does not require the use of advanced track tracing algorithms (e.g., Lampert and O'Keefe, 2010). For the applications where the ENF needs to be eliminated from the data, subtraction algorithms (Butler and Russell, 1993, 2003) may benefit from using reference ENF data too. This is particularly true for extremely (ELF) and very low frequency (VLF) radio data between 300 to 30 000 Hz (Cohen et al., 2010), since the affected bandwidth of the ENF fluctuations grows proportionally with higher overtones. With reference data, the ENF can be specifically targeted and generic bandstop filters can be avoided.

Cross correlations between estimated and reference ENF data provide a reliable, passive technique for the detection of timing anomalies in geophysical data. However, the limitations of the method are clear: the reliability of the timing corrections is contingent on the ability to accurately resolve the ENF signal from the data, which is not always easily achieved. The expected precision and accuracy of the technique illustrated in fig. 6 and reaches approximately $1\,\mathrm{s}$ for instruments that express a high susceptibility to the ENF. By increasing the sampling resolution of the reference ENF data, time discrepancies on the sub-second level may potentially be discovered. During the analysis of the teleseismic event (fig. 7) it was found that there was a consistent delay ($6\,\mathrm{s}$) with the reference ENF for the entire NSAN. This delay is not real considering most of the stations are GPS locked and show $0\,\mathrm{s}$ delays during other periods. It is expected that this effect may be introduced by poor timing quality of the reference ENF data itself, or potentially by another unknown cause that needs to be investigated further. A similar explanation concerning inaccurate timestamping of the reference ENF data may also explain the skew towards $-1\,\mathrm{s}$ in fig. 6. It should be noted that if the absolute timestamp of the reference data is inaccurate, relative timing differences between instruments using the ENF remain resolvable.

Results from the polarization analysis (figs. 8 and 9) shows that gross orientation anomalies can be successfully identified. Even if the source of the ENF signal is unknown, when the source remains stable through time (e.g., a non-mobile transformer or the installation cabinet), the rectilinearity of geophysical data at the ENF

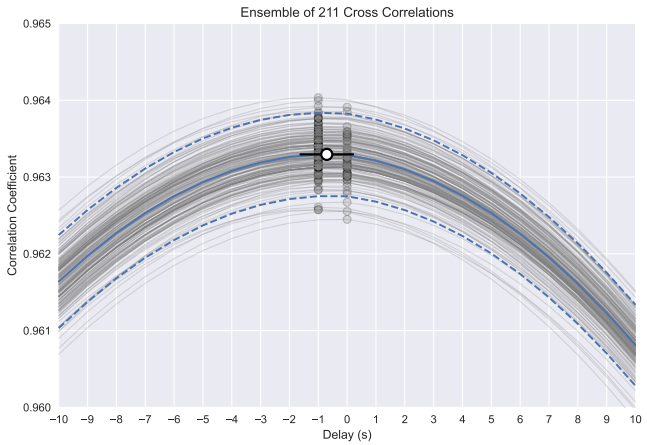

Figure 6 Average and 95 % confidence limits (blue curves) of an ensemble of 211 cross correlations with the measured ENF (grey curves) for all components of all Groningen surface accelerometer in the G-network on 2020-03-01. The accelerometer data have accurate timestamps and should resolve to a zero-time delay. The grey markers indicate the recovered peaks from the cross correlations and hence the respective delay times with the measured ENF. The black marker represents the mean time lag and 95 % confidence interval, illustrating the accuracy and precision of the method approaches 1 s.

may thus provide a reasonable tool for the detection of temporal instrumental orientation anomalies. Furthermore, this method may provide a tool to more accurately determine three-dimensional orientations of geophones installed in seismic boreholes that needs to be investigated. Perhaps, even small orientation anomalies may be discovered that are on the order a few degrees.

5.1 Source of the ENF in Geophysical Data

The mechanisms through which the ENF signal is passed on to geophysical sensor networks remains enigmatic and appears to vary per instrument type and installation (fig. 1). In the following section, the expected sources in the different geophysical instruments are discussed. Because of the alternative suspected coupling mechanism, acoustic instruments are treated in the supplementary information.

5.1.1 G-network Accelerometers and Geophones

From the presented polarization analysis it is evident that the ENF signal is acquired locally in the G-network accelerometers. Despite this, in the operational NSAN, a sudden increase in the amplitude of the ENF has been observed to lead to false event detection in accelerometers deployed near high voltage power lines – suggesting that large-scale electrical infrastructure may under certain circumstances be a significant source of the ENF signal. Seismoacoustic coupling (e.g., Evers et al., 2007) from humming and corona discharge (Loeb, 1965) may provide a coupling mechanism up to 200 m away from high voltage power lines (Schippkus et al., 2020). The susceptibility of the G-network accelerometers to the ENF is strong and highly polarized. It is expected that the signal would be less dominant if it were induced along the wires between the sensor and digitizer where it is not amplified to such dominant amplitudes. Furthermore, accelerometers in the NSAN are connected with a two-wire differential setup, effectively limiting the influence of external magnetic fields on grounds loops specifically, but leaving the sensor itself susceptible to changing magnetic fields. The recorded power at the ENF in accelerometers with different gain settings and sensitivities appears similar across the G-network when the amplitude of the signal is expressed in physical ground motion units (acceleration, velocity, or displacement), suggesting that the ENF signal is not electromagnetic of nature. Alterations in the suspension spring or coils of the accelerometers (Forbriger, 2007) have been suggested as a likely source of the signal. The relationship between the cabinet orientation and the polarization azimuth of the accelerometer data indicates that physical vibration of the cabinet itself may be caused by the humming power supply that is mounted on its inside wall.

The geophones inside the seismic boreholes of the G-network share surface electronics with the aforementioned accelerometers. The geophones operate passively and have no direct power source but are connected to the power grid through a digitizer at the surface. The amplitude of the ENF in these data is orders of magnitude smaller compared to the accelerometers and show varying directions of polarization within a single borehole. The polarization is strong, yet orientations vary unpredictably over the 50 m depth levels inside the borehole, and because no decrease with depth inside the boreholes (from 50 to 200 m) could be identified, it is suggested that the ENF signal is potentially established at the surface. For these instruments, it may be that unshielded signal cables connected to the datalogger allow for direct induction of stray magnetic fields from nearby electrical components. A more thorough assessment of the ENF signal in geophones inside the seismic boreholes is recommended.

5.1.2 E-TEST Battery Operated Geophones

Surface geophones from the E-TEST temporary deployment (Shahar Shani-Kadmiel et al., 2020) are fully battery operated and enclosed within a single unit. These instruments are of interest because they have no physical connection to the electrical grid. For these geophones, the ENF signal is only detectable and usable when the instruments are deployed near towns (fig. 10), visible overhead power lines, or sub-surface electrical infrastructure, as revealed by the presence of e.g., street lights. In the middle of a forest or field, the ENF signal could not be recovered from the data. It is still unknown whether the coupling is purely electromagnetic or through (coupled) waves as a result of the humming and vibration of the nearby electrical components.

5.2 Further Applications of ENF Analysis

In the previous sections, the benefits and versatile application of ENF analysis in the passive quality assessment

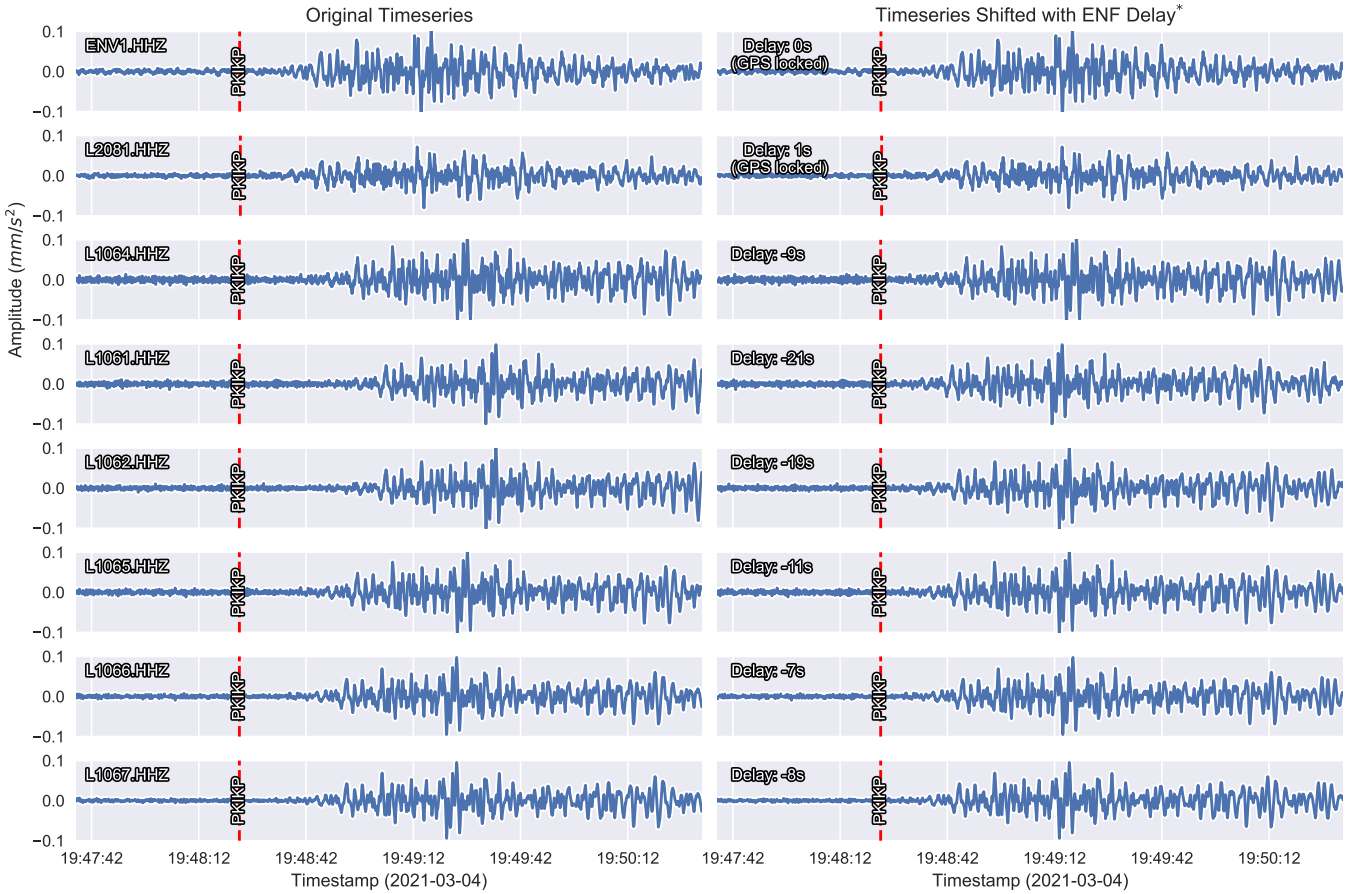

Figure 7 Comparison of GPS locked station with near zero delay (ENV1, L2081) with local array L106 (bottom 6 rows) recording a teleseismic arrival. The expected arrival times for PKIKP phase is illustrated. The right columns shows the same traces shifted by the recovered timing error from the ENF analysis. *Note: all delays were corrected for a consistent $-6\,\mathrm{s}$ offset across the entire network that appeared present on that day.

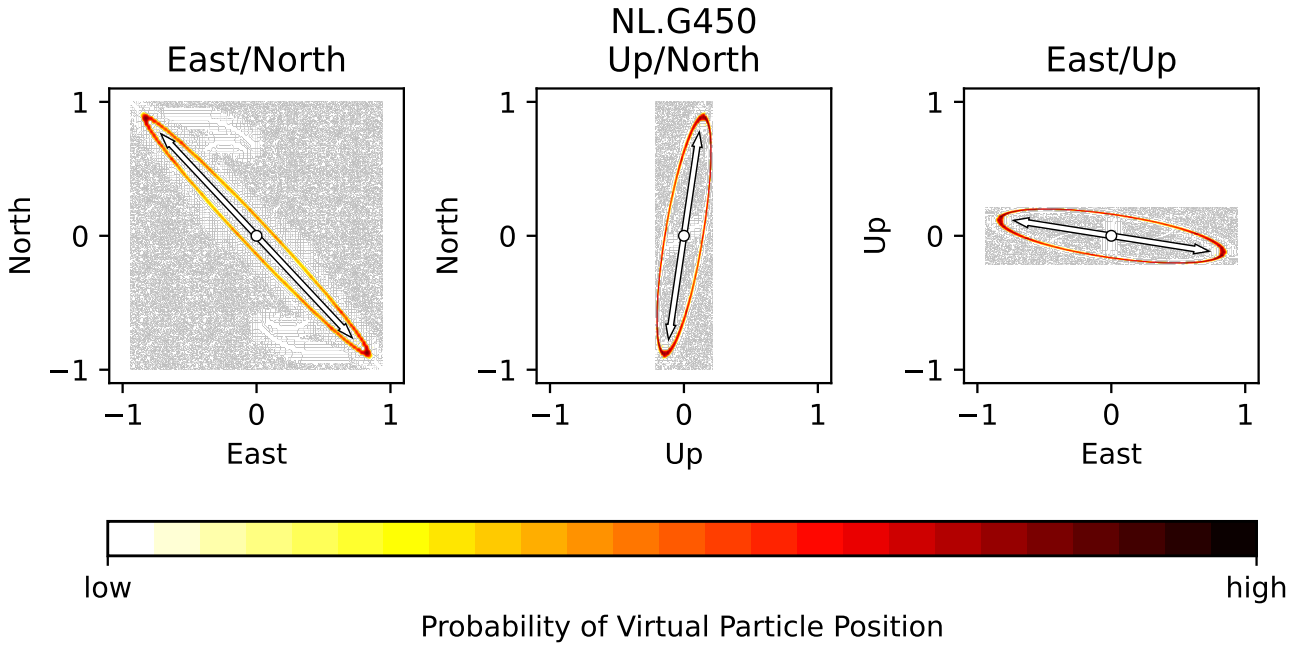

Figure 8 Strongly polarized motion at the ENF (bandpassed 49.85 to $50.15\,\mathrm{Hz}$) for surface accelerometer G450 (2020-03-01 – 2020-03-02). The three panels show 2-dimensional probabilistic histograms of the particle motion in East/North, Up/North, and East/Up directions, respectively. The white arrows with black outline represent the geographic orientation of the largest principal component ($\mathbf{u}_1$) that is equal to the direction of dominant particle motion. The leftmost panel can be interpreted as the geographical azimuth of dominant motion.

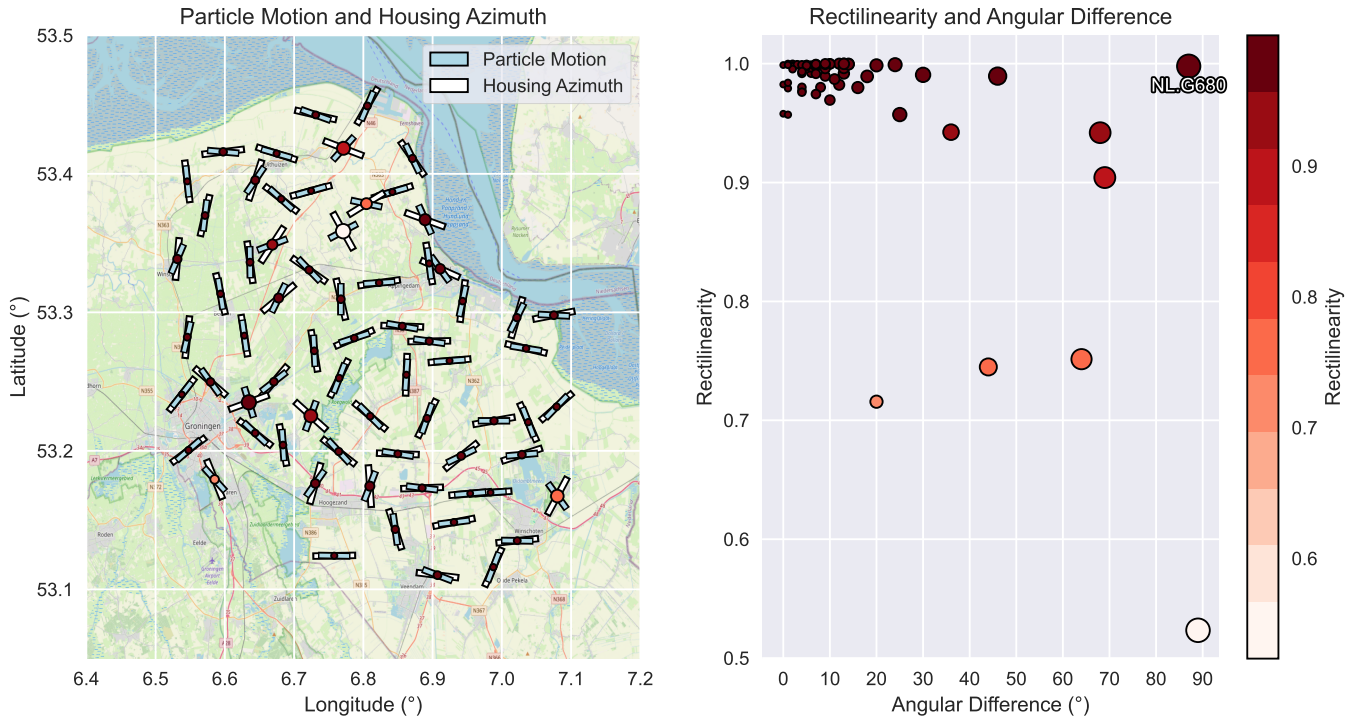

Figure 9 **Left:** comparison between azimuths of the principal direction of accelerometer particle motion (lightblue) and the orientation of the installation cabinet (white). **Right:** Angular misfit between the cabinet orientation and dominant particle motion against the degree of rectilinearity. Map data are provided by OpenStreetMap contributors (2017).

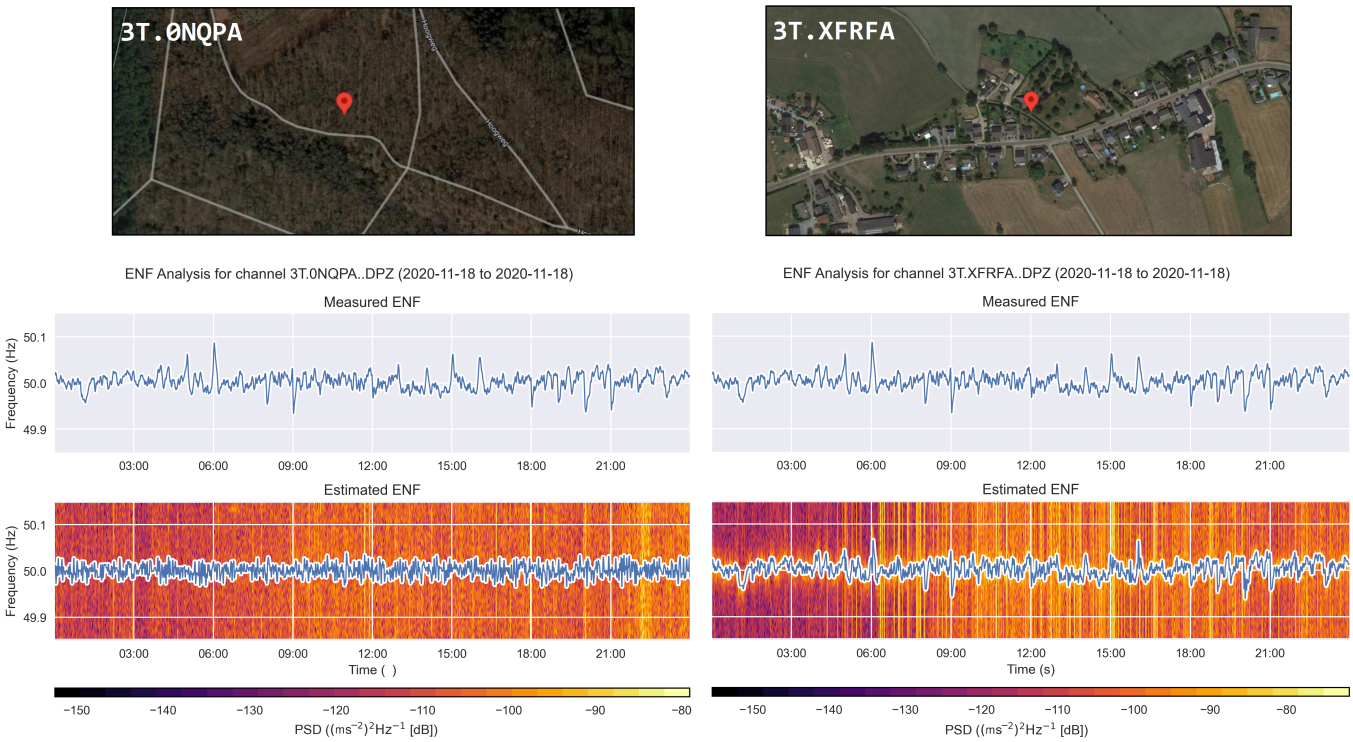

Figure 10 Columns showing two battery operated geophones in the 3T temporary deployment (Shahar Shani-Kadmiel et al., 2020). The left column shows geophone node 0NQPA remotely deployed in a forest and shows no trace of the ENF in its data. The right column represents data from geophone node XFRFA which is located near a town and electrical infrastructure. The ENF signal is clearly derived from anthropgenic activity in this area.

of geophysical data was demonstrated. Because the signal is persistent and omnipresent, some other foreseeable applications and possibilities for future consideration are discussed below.

Seismometers are considered to be linear time-invariant (LTI) systems. This description implies that an input of particular frequency should output a signal with equal frequency, albeit with modified ampli-

tude and phase, as described by the instrument's transfer function. Because the input signal of the ENF is well-defined and predictable, its characteristics should be accurately reflected in the output signal. A number of LOFAR stations in the NSAN network show an anomalous consistent positive shift in the ENF of 0.01 Hz. This feature may represent a deviation from a linear response, or that there exists a minor drift in the clock that may stretch sample spacing, providing the appearance of a higher frequency input signal. The latter hypothesis seems most likely considering the stations are known to use non-commercial dataloggers.

Additionally, the absolute (integrated) amount of power of the observed ENF in digital recordings varies significantly as a function of time. Many features are expressed in this variation, most of which do not yet have identified sources. The most coherent changes happen on timescales of minutes to days and occur simultaneously and proportionally between all stations in the network. Diurnal variation of the strength of the ENF signal appears to be to some degree coherent with measures of the consumer load. An in-depth investigation on these varying amplitude, including a better understanding of coupling mechanisms in geophysical instruments, may provide opportunities for other potential benefits of ENF analysis to be identified, such as the potential detection of sensitivity anomalies. Furthermore, the coherency of the varying ENF signal strength between stations may provide an alternative way to detect relative timing issues that needs to be investigated.

6 Conclusion

The application of ENF analysis to the passive quality assessment of geophysical data is a versatile technique that can be leveraged to identify timing issues at the 1 s level. It is also demonstrated that a polarization analysis of accelerometer data at the ENF enabled instrumentation orientation errors to be detected and resolved. ENF analysis may thus be considered for the passive detection of timing errors and sensor orientation anomalies, and in data where the provided timestamp may be tampered with, or generally unreliable, for example due to the lack of GPS connectivity. The mechanism through which the ENF is coupled to geophysical data appears to be instrument and installation specific and needs to be investigated further. Despite this, the proposed methods can potentially be adopted by geophysical monitoring institutes, and opens multiple avenues for further research.

Acknowledgements

We are grateful for our dear colleagues at the Seismology and Acoustics department at KNMI for their fruitful comments and assistance. Two anonymous reviewers are thanked for providing their input on the manuscript and suggestions to improve its clarity. We thank Carrick Talmadge for discussions on the detection of 100 Hz signals on low-frequency sound microphones. Henrietta Rákóczi is thanked for her input on the sections of the manuscript that were considered redundant and could be removed. L. Gorjão is thanked for an interesting discussion on power-grid dynamics and their effort in the creation and maintenance of the power-grid frequency database. This work was initially inspired by a science video created by Tom Scott on the electrical network frequency.

Data and code availability

Reference ENF data were downloaded from the power-grid frequency database (Gorjão et al., 2020) and the TransnetBW GmBH website that is accessible at https://www.transnetbw.com. Seismological waveform data were downloaded from the Netherlands Seismic Acoustic Network (KNMI, 1993) and the E-TEST deployment (Shahar Shani-Kadmiel et al., 2020). The ENF analysis script was written in Python 3.8.2 (Van Rossum and Drake, 2009), using SciPy (Virtanen et al., 2020) and NumPy (Harris et al., 2020). Figures were made with Matplotlib (Hunter, 2007), version 3.2.1 (Caswell et al., 2020) and a pre-release version of PyGMT (Uieda et al., 2021) using Generic Mapping Tools (GMT) version 6 (Wessel et al., 2019b,a). Electrical infrastructure data were downloaded from the Enexis homepage (https://www.enexis.nl/) and TenneT homepage (https://www.tennet.eu).

Competing interests

The authors declare no competing interests.

References

Ahern, T., Benson, R., Casey, R., Trabant, C., and Weertman, B. Improvements in Data Quality, Integration and Reliability: New Developments at the IRIS DMC. *Advances in Geosciences*, 40: 31–35, 2015. doi: 10.5194/adgeo-40-31-2015.

Beyreuther, M., Barsch, R., Krischer, L., Megies, T., Behr, Y., and Wassermann, J. ObsPy: A Python toolbox for seismology. *Seismological Research Letters*, 81(3):530–533, 2010. doi: 10.1785/gssrl.81.3.530.

Bormann, P. and Wielandt, E. Seismic signals and noise. In *New Manual of Seismological Observatory Practice 2 (NMSOP2)*, pages 1–62. Deutsches GeoForschungsZentrum GFZ, 2013. doi: 10.2312/GFZ.NMSOP-2_ch4.

Butler, K. E. and Russell, R. D. Subtraction of powerline harmonics from geophysical records. *Geophysics*, 58(6):898–903, 1993. doi: 10.1190/1.1443474.

Butler, K. E. and Russell, R. D. Cancellation of multiple harmonic noise series in geophysical records. *Geophysics*, 68(3): 1083–1090, 2003. doi: 10.1190/1.1581080.

Caswell, T. A., Droettboom, M., Lee, A., Hunter, J., Firing, E., Stansby, D., Klymak, J., Hoffmann, T., de Andrade, E. S., Varoquaux, N., Nielsen, J. H., Root, B., Elson, P., May, R., Dale, D., Lee, J.-J., Seppänen, J. K., McDougall, D., Straw, A., Hobson, P., Gohlke, C., Yu, T. S., Ma, E., Vincent, A. F., Silvester, S., Moad, C., Kniazev, N., Ivanov, P., Ernest, E., and Katins, J. matplotlib/matplotlib: REL: v3.2.1. doi: 10.5281/zenodo.3714460.

Cohen, M. B., Said, R., and Inan, U. Mitigation of 50–60 Hz power line interference in geophysical data. *Radio Science*, 45(06): 1–12, 2010. doi: 10.1029/2010RS004420.

Cooper, A. H. The electric network frequency (ENF) as an aid to authenticating forensic digital audio recordings – an automated approach. *Journal of the Audio Engineering Society*, 2008.

Cooper, A. J. An automated approach to the Electric Network Frequency (ENF) criterion - Theory and practice. *International Journal of Speech Language and the Law*, 16(2), 2010. doi: 10.1558/ijsll.v16i2.193.

Coyne, J., Bobrov, D., Bormann, P., Duran, E., Grenard, P., Haralabus, G., Kitov, I., and Starovoit, Y. CTBTO: Goals, networks, data analysis and data availability. In *New manual of seismological observatory practice 2 (NMSOP-2)*, pages 1–41. Deutsches GeoForschungsZentrum GFZ, 2012. doi: 10.2312/GFZ.NMSOP-2_ch15.

Evers, L. G., Ceranna, L., Haak, H. W., Pichon, A. L., and Whitaker, R. W. A seismoacoustic analysis of the gas-pipeline explosion near Ghislenghien in Belgium. *Bulletin of the Seismological Society of America*, 97(2):417–425, 2007. doi: 10.1785/0120060061.

Forbriger, T. Reducing magnetic field induced noise in broad-band seismic recordings. *Geophysical Journal International*, 169(1): 240–258, 2007. doi: 10.1111/j.1365-246X.2006.03295.x.

Gange, M. Low-frequency and tonal characteristics of Transformer noise. In *Proceedings of Acoustics*, 2011.

Garg, R., Varna, A. L., and Wu, M. "Seeing" ENF: Natural time stamp for digital video via optical sensing and signal processing. In *Proceedings of the 19th ACM International Conference on Multimedia*, MM '11, page 23–32. Association for Computing Machinery, 2011. doi: 10.1145/2072298.2072303.

Garg, R., Varna, A. L., and Wu, M. Modeling and analysis of electric network frequency signal for timestamp verification. In *2012 IEEE International Workshop on Information Forensics and Security (WIFS)*, pages 67–72. IEEE, 2012. doi: 10.1109/WIFS.2012.6412627.

Gorjão, L. R., Jumar, R., Maass, H., Hagenmeyer, V., Yalcin, G. C., Kruse, J., Timme, M., Beck, C., Witthaut, D., and Schäfer, B. Open database analysis of scaling and spatio-temporal properties of power grid frequencies. *Nature communications*, 11(1):1–11, 2020. doi: 10.1038/s41467-020-19732-7.

Harris, C. R., Millman, K. J., van der Walt, S. J., Gommers, R., Virtanen, P., Cournapeau, D., Wieser, E., Taylor, J., Berg, S., Smith, N. J., Kern, R., Picus, M., Hoyer, S., van Kerkwijk, M. H., Brett, M., Haldane, A., del Río, J. F., Wiebe, M., Peterson, P., Gérard-Marchant, P., Sheppard, K., Reddy, T., Weckesser, W., Abbasi, H., Gohlke, C., and Oliphant, T. E. Array programming with NumPy. *Nature*, 585(7825):357–362, 2020. doi: 10.1038/s41586-020-2649-2.

Hunter, J. D. Matplotlib: a 2D graphics environment. *Computing in Science & Engineering*, 9(3):90–95, 2007. doi: 10.1109/MCSE.2007.55.

Imanishi, Y., Nawa, K., Tamura, Y., and Ikeda, H. Effects of vertical nonlinearity on the superconducting gravimeter CT# 036 at Ishigakijima, Japan. *Earth, Planets and Space*, 74(1):1–15, 2022. doi: 10.1186/s40623-022-01609-2.

Jurkevics, A. Polarization analysis of three-component array data. *Bulletin of the seismological society of America*, 78(5):1725–1743, 1988. doi: 10.1785/BSSA0780051725.

Kennett, B. and Engdahl, E. Traveltimes for global earthquake location and phase identification. *Geophysical Journal International*, 105(2):429–465, 1991. doi: 10.1111/j.1365-246X.1991.tb06724.x.

Klun, M., Zupan, D., Lopatič, J., and Kryžanowski, A. On the Application of Laser Vibrometry to Perform Structural Health Monitoring in Non-Stationary Conditions of a Hydropower Dam. *Sensors*, 19(17):3811, 2019. doi: 10.3390/s19173811.

KNMI. Netherlands Seismic and Acoustic Network. Royal Netherlands Meteorological Institute (KNMI), Other/Seismic Network, 1993. doi: 10.21944/e970fd34-23b9-3411-b366-e4f72877d2c5.

Koymans, M., Domingo Ballesta, J., Ruigrok, E., Sleeman, R., Trani, L., and Evers, L. Performance assessment of geophysical instrumentation through the automated analysis of power spectral density estimates. *Earth and Space Science*, 8(9): e2021EA001675, 2021. doi: 10.1029/2021EA001675.

Křen, P., Pálinkáš, V., Val'ko, M., and Mašika, P. Improved measurement model for FG5/X gravimeters. *Measurement*, 171:108739, 2021. doi: 10.1016/j.measurement.2020.108739.

Lampert, T. A. and O'Keefe, S. E. A survey of spectrogram track detection algorithms. *Applied acoustics*, 71(2):87–100, 2010. doi: 10.1016/j.apacoust.2009.08.007.

Levkov, C., Mihov, G., Ivanov, R., Daskalov, I., Christov, I., and Dotsinsky, I. Removal of power-line interference from the ECG: a review of the subtraction procedure. *BioMedical Engineering OnLine*, 4(1):1–18, 2005. doi: 10.1186/1475-925X-4-50.

Loeb, L. B. *Electrical coronas, their basic physical mechanisms*. Univ of California Press, 1965.

McNamara, D. and Boaz, R. PQLX: A software tool to evaluate seismic station performance. In *AGU Fall Meeting Abstracts*, 2006.

OpenStreetMap contributors. Planet dump retrieved from https://planet.osm.org. https://www.openstreetmap.org, 2017.

Pedersen, H. A., Leroy, N., Zigone, D., Vallée, M., Ringler, A. T., and Wilson, D. C. Using Component Ratios to Detect Metadata and Instrument Problems of Seismic Stations: Examples from 18 Yr of GEOSCOPE Data. *Seismological Research Letters*, 91(1): 272–286, 2020. doi: 10.1785/0220190180.

Petersen, G. M., Cesca, S., and and, M. K. Automated Quality Control for Large Seismic Networks: Implementation and Application to the AlpArray Seismic Network. *Seismological Research Letters*, 90(3):1177–1190, 2019. doi: 10.1785/0220180342.

Raspberry Shake, S.A. Raspberry Shake, 2016. doi: 10.7914/SN/AM.

Ringler, A. T., Hagerty, M., Holland, J., Gonzales, A., Gee, L. S., Edwards, J., Wilson, D., and Baker, A. The data quality analyzer: A quality control program for seismic data. *Computers & Geosciences*, 76:96–111, 2015. doi: 10.1016/j.cageo.2014.12.006.

Schippkus, S., Garden, M., and Bokelmann, G. Characteristics of the Ambient Seismic Field on a Large-N Seismic Array in the Vienna Basin. *Seismological Research Letters*, 91(5):2803–2816, 2020. doi: 10.1785/0220200153.

Shahar Shani-Kadmiel, Frank Linde, Läslo Evers, and Bjorn Vink. Einstein Telescope Seismic Campaigns, 2020. doi: 10.7914/SN/3T_2020.

Trani, L., Koymans, M., Atkinson, M., Sleeman, R., and Filgueira, R. WFCatalog: A catalogue for seismological waveform data. *Computers & Geosciences*, 106:101–108, 2017. doi: 10.1016/j.cageo.2017.06.008.

Uieda, L., Tian, D., Leong, W., Toney, L., Schlitzer, W., Grund, M., Newton, D., Ziebarth, M., Jones, M., and Wessel, P. PyGMT: A Python interface for the Generic Mapping Tools. 2021. doi: 10.5281/zenodo.7772533.

Van Rossum, G. and Drake, F. L. *Python 3 Reference Manual*. CreateSpace, Scotts Valley, CA, 2009.

Virtanen, P., Gommers, R., Oliphant, T. E., Haberland, M., Reddy, T., Cournapeau, D., Burovski, E., Peterson, P., Weckesser, W., Bright, J., van der Walt, S. J., Brett, M., Wilson, J., Millman, K. J., Mayorov, N., Nelson, A. R. J., Jones, E., Kern, R., Larson, E., Carey, C. J., Polat, İ., Feng, Y., Moore, E. W., VanderPlas, J., Laxalde, D., Perktold, J., Cimrman, R., Henriksen, I., Quintero, E. A.,

Harris, C. R., Archibald, A. M., Ribeiro, A. H., Pedregosa, F., van Mulbregt, P., and SciPy 1.0 Contributors. SciPy 1.0: Fundamental Algorithms for Scientific Computing in Python. *Nature Methods*, 17:261–272, 2020. doi: 10.1038/s41592-019-0686-2.

Wessel, P., Luis, J., Uieda, L., Scharroo, R., Wobbe, F., Smith, W. H., and Tian, D. The Generic Mapping Tools version 6. *Geochemistry, Geophysics, Geosystems*, 20(11):5556–5564, 2019a. doi: 10.1029/2019GC008515.

Wessel, P., Luis, J. F., Uieda, L., Scharroo, R., Wobbe, F., Smith, W. H. F., and Tian, D. The Generic Mapping Tools version 6. doi: 10.5281/zenodo.3407866. Funded by US National Science Foundation grants OCE-1558403 and EAR-1829371.

Xia, J. and Miller, R. D. Design of a hum filter for suppressing powerline noise in seismic data. *Journal of Environmental & Engineering Geophysics*, 5(2):31–38, 2000. doi: 10.4133/JEEG5.2.31.